Fabrication of Mesoporous CdTe/ZnO@SiO_2 Core/Shell Nanostructures with Tunable Dual Emission and Ultrasensitive Fluorescence Response to Metal Ions

Yingying Song,[†] Xuebo Cao,*[,†] Yang Guo,[†] Peng Chen,[†] Qingrui Zhao,[‡] and Guozhen Shen*[,§]

Key Laboratory of Organic Synthesis of Jiangsu Province and Department of Chemistry, Suzhou University, Suzhou, Jiangsu 215123, China, Beijing Research Institute of Chemical Industry, SINOPEC, China, and Department of Electrical Engineering, University of Southern California, Los Angeles, California 90089

Received July 14, 2008. Revised Manuscript Received October 5, 2008

In this paper, we demonstrated the encapsulation of CdTe quantum dots (QDs) and ZnO nanorods (NRs) with a layer of mesoporous SiO_2 shell (pore size: 4.1 nm) for the purpose of integrating dual-emission property into one common nanostructure. Within the core−shell CdTe/ZnO@SiO_2 nanocomposites, CdTe QDs and ZnO NRs provide visible emission and UV emission, respectively. The fluorescence intensity ratio of the dual emission can be tuned by altering the hydrolysis time of tetraethyl orthosilicate (TEOS). The core−shell CdTe/ZnO@SiO_2 nanocomposites exhibit very interesting photoluminescent behaviors after interactions with heavy-metal ions such as Hg^{2+}, Pb^{2+}, and Cu^{2+}. The visible emission contributed by CdTe QDs was abnormally enhanced in a range of 20−90% at the concentration of $Hg^{2+} < 10^{-8}$ M, $Pb^{2+} < 10^{-5}$ M, and $Cu^{2+} < 10^{-6}$ M, whereas the intensity of UV emission by ZnO NRs was kept constant in all cases. Consequently, the UV emission may serve as a reference. The mechanism of the fluorescence enhancement is presumed to be the adsorption of the metal ions by the trap sites and the resulting surface passivation of the QDs. The mesoporous silica shell of the nanocomposites also plays a key role in the process of fluorescence enhancement, which helps to protect the surface characteristics of QDs, prevent the flocculation of the particles, and promote the adsorption of Cu^{2+}, Hg^{2+}, and Pb^{2+} ions. The variable visible emission in combination with the constant UV emission indicates that the as-prepared CdTe/ZnO@SiO_2 core/shell nanostructures may serve as novel biluminescent materials as well as reliable and sensitive fluorescence probes.

Introduction

Currently, the fabrication of composite nanostructures using the preformed nanocrystals as building blocks is of great interests because it can integrate several different functionalities required by the applications into one common nanostructure.[1] Attracted by their strong, tunable photoluminescence (PL) in a range of wavelengths, Cd chalcogenide (CdX, X = S, Se, and Te) quantum dots (QDs) were widely used in the preparation of various composite nanostructures. Frequently, QDs together with magnetic nanoparticles were intercalated into silica or polystyrene microbeads for biological applications, in which QDs act as fluorescent probes and magnetic nanoparticles as controlled transport platforms.[2] Besides serving as key components of magnetic-fluorescent nanocomposites, QDs binding onto semiconductor nanocrystals to form semiconductor/semiconductor heterostructures are also attractive. For instance, CdSe and CdTe QDs have been deposited onto the surfaces of TiO_2 nanowires and nanoribbons,[3,4] ZnO nanorods,[5] and Cu_3Se_2 nanoplates[6]

* Corresponding authors. E-mail: xbcao@suda.edu.cn (X.C.); guozhens@usc.edu (G.S.).
[†] Suzhou University.
[‡] Beijing Research Institute of Chemical Industry.
[§] University of Southern California.

(1) (a) Shen, G. Z.; Bando, Y.; Ye, C. H.; Yuan, X. L.; Sekiguchi, T.; Golberg, D. *Angew. Chem., Int. Ed.* **2006**, *45*, 7568. (b) Cao, X. B.; Gu, L.; Zhuge, L. J.; Gao, W. J.; Wang, W. C.; Wu, S. F. *Adv. Funct. Mater.* **2006**, *16*, 896. (c) Cao, X. B.; Lan, X. M.; Guo, Y.; Zhao, C.; Han, S. M.; Wang, J.; Zhao, Q. R. *J. Phys. Chem. C* **2007**, *111*, 18958. (d) Mokari, T.; Rothenberg, E.; Popov, I.; Costi, R.; Banin, U. *Science* **2004**, *304*, 1787. (e) Li, Y.; Zhang, Q.; Nurmikko, A. V.; Sun, S. *Nano Lett.* **2005**, *5*, 1689. (f) Pellegrino, T.; Fiore, A.; Carlino, E.; Giannini, C.; Cozzoli, P. D.; Ciccarella, G.; Respaud, M. L.; Cingolani, R.; Manna, L. *J. Am. Chem. Soc.* **2006**, *128*, 6690. (g) Robel, I.; Bunker, B. A.; Kamat, P. V. *Adv. Mater.* **2005**, *17*, 2458.

(2) (a) Kim, J.; Lee, L. E.; Lee, J.; Yu, J. H.; Kim, B. C.; An, K.; Hwang, Y.; Shin, C. H.; Park, J. G.; Kim, J.; Hyeon, T. *J. Am. Chem. Soc.* **2006**, *128*, 688. (b) Wang, G. P.; Song, E. Q.; Xie, H. Y.; Zhang, Z. L.; Tian, Z. Q.; Zuo, C.; pang, D. W.; Wu, D. C.; Shi, Y. B. *Chem. Commun.* **2005**, 4276. (c) Gu, H.; Zheng, R.; Zhang, X. X.; Xu, B. *J. Am. Chem. Soc.* **2004**, *126*, 5664. (d) Kim, H.; Achermann, M.; Balet, L. P.; Hollingsworth, J. A.; Klimov, V. I. *J. Am. Chem. Soc.* **2005**, *127*, 544. (e) Yi, D. K.; Selvan, S. T.; Lee, S. S.; Papaefthymiou, G. C.; Kundaliya, D.; Ying, J. Y. *J. Am. Chem. Soc.* **2005**, *127*, 4990. (f) Wang, D. S.; He, J. B.; Rosenzweig, N.; Rosenzweig, Z. *Nano Lett.* **2004**, *4*, 409.

(3) Lee, J. C.; Sung, Y. M.; Kim, T. G.; Choi, H. J. *Appl. Phys. Lett.* **2007**, *91*, 113104.

(4) (a) Chong, S. V.; Suresh, N.; Xia, J.; Al-Salim, N.; Idriss, H. *J. Phys. Chem. C* **2007**, *111*, 10389. (b) Gunes, S.; Neugebauer, H.; Sariciftci, N. S.; Roither, H.; Kovalenko, M.; Pillwein, G.; Heiss, W. *Adv. Funct. Mater.* **2006**, *16*, 1095.

(5) (a) Tena-Zaera, R.; Katty, A.; Bastide, S.; Lévy-Clément, C. *Chem. Mater.* **2007**, *19*, 1626. (b) Lévy-Clément, C.; Tena-Zaera, R.; Ryan, M. A.; Katty, A.; Hodes, G. *Adv. Mater.* **2005**, *17*, 1512. (c) Kim, J. Y.; Osterloh, F. E. *J. Am. Chem. Soc.* **2007**, *127*, 10152.

(6) Cao, X. B.; Zhao, C.; Lan, X. M.; Gao, W. J.; Qian, W. H.; Guo, Y. *J. Phys. Chem. C* **2007**, *111*, 6658.

10.1021/cm801925j CCC: $40.75
Published on Web 12/03/2008

through electrostatic interactions, ligand exchanges, or chemical vapor depositions. These studies mainly took advantage of the good visible light-absorbing effect of QDs and their ability to generate multiple electron−hole pairs per photon,[7] which could efficiently improve the photovoltaic performances of the modified semiconductors. However, the intrinsic PL properties of QDs modified semiconductor nanocomposites were generally ignored in these studies.[8] In fact, due to the contribution by QDs and the semiconductor capable of photoluminescence, biluminescent property may be observed in them.

Nanomaterials with dual emission are widely applied in the fields of biluminescence,[9] multiplex signaling,[10] dual labeling, and detection.[11] Especially, it will be ideal if one of the emission bands can keep constant intensity in the process of fluorescence sensing, which is because the indication of the amount of the object detected with the fluorescence intensity ratio of the dual emission will be more reliable and precise compared to the fluorescence sensing with the absolute fluorescence intensity in single-emission materials.[12,13] Generally, dual emission is observed in organic and complex materials containing two different emissive species. Some single-component inorganic nanocrystals such as ZnO and ZnS also exhibit biluminescent properties: one originates from the excitonic recombination and the other is defect-related.[14,15] Taking ZnO nanocrystals as an example, their PL spectrum typically features a narrow UV excitonic emission band (∼384 nm) and a broadband in the visible region (∼580 nm) attributing to the recombination of an electron with a hole at a defect site. Of course, ZnO nanocrystals exhibiting only excitonic emission can also be achieved by finely regulating experimental conditions.[16] The excitonic emission is a desired physical property of ZnO that can be applied in various UV nanodevices, whereas sometimes the visible emission was not expected because it was defect-related and its intensity and position were not easily manipulated. As mentioned above, composite nanostructures can exhibit the properties of all components within them and CdX QDs possess size-dependent emission with high PL quantum yields. Consequently, if ZnO nanocrystals with pure excitonic emission are preprepared and then combined with CdX QDs, the resulting nanostructures will exhibit both UV emission and tunable visible emission, which should be superior to dually emissive organic and complex materials and single-component inorganic nanocrystals in the good photostability, controllable photoluminescence, and narrow emission bandwidth.

Scheme 1. Schematic Description of CdTe/ZnO@SiO$_2$ Core/Shell Nanostructures

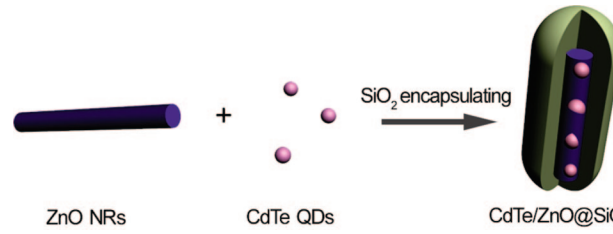

Building from these ideas, here we first prepared colloidal, monodispersed ZnO nanorods (NRs) with pure excitonic emission by reacting zinc acetate with potassium hydroxide in methanol, and then applied SiO_2 as the encapsulation agent to package ZnO NRs and CdTe QDs into one common nanostructure, resulting in water-soluble, mesoporous CdTe/ZnO@SiO_2 core/shell nanostructures with tunable dual emission (Scheme 1). The mesoporous SiO_2 shells of the nanocomposites not only seal CdTe QDs inside the nanocomposites but also allow the entering of small molecules and ions to contact with the QDs to cause a fluorescence response. ZnO NRs and CdTe QDs embedded within the silica shell impart UV emission and tunable visible emissions to the nanocomposites, respectively. Surprisingly, the visible emission contributed by CdTe QDs in CdTe/ZnO@SiO_2 core/shell nanostructures was found to exhibit abnormal enhancement when the nanocomposites were incubated with trace Cu^{2+}, Hg^{2+}, or Pb^{2+} ions, which is quite different from previous reports that these heavy-metal ions are effective quenchers of the fluorescence of CdTe QDs.[17−22] Moreover,

(7) (a) Schaller, R. D.; Klimov, V. I. *Phys. Rev. Lett.* **2004**, *92*, 186601. (b) Ellingson, R. J.; Beard, M. C.; Johnson, J. C.; Yu, P. R.; Micic, O. I.; Nozik, A. J.; Shabaev, A.; Efros, A. L. *Nano Lett.* **2005**, *5*, 865.
(8) (a) Battaglia, D.; Blackman, B.; Peng, X. G. *J. Am. Chem. Soc.* **2005**, *127*, 10889. (b) Chen, C. C.; Yet, C. P.; Wang, H. N.; Chao, C. Y. *Langmuir* **1999**, *15*, 6845. (c) Nizamoglu, S.; Mutlugun, E.; Ozel, T.; Demir, H. V.; Sapra, S.; Gaponik, N.; Eychmuller, A. *Appl. Phys. Lett.* **2008**, *92*, 113110. (d) Pradhan, N.; Efrima, S. *J. Am. Chem. Soc.* **2003**, *125*, 2050.
(9) (a) Wang, L.; Yang, C. Y.; Tan, W. H. *Nano Lett.* **2005**, *5*, 37. (b) Wenger, J.; Gerard, D.; Lenne, P. F.; Rigneault, H.; Dintinger, J.; Ebbesen, T. W.; Boned, A.; Conchonaud, F.; Marguet, D. *Opt. Express* **2006**, *14*, 12206.
(10) (a) Hochreiner, H.; Sanchez-Barragan, I.; Costa-Fernandez, J. M.; Sanz-Medel, A. *Talanta* **2005**, *66*, 611. (b) Im, S. H.; Khalil, G. E.; Callis, J.; Ahn, B. H.; Gouterman, M.; Xia, Y. N. *Talanta* **2005**, *67*, 492. (c) Zhu, L. Y.; Wu, W. W.; Zhu, M. Q.; Han, J. J.; Hurst, J. K.; Li, A. D. Q. *J. Am. Chem. Soc.* **2007**, *129*, 3524. (d) Kim, H.-J.; Lee, J.; Kim, T. H.; Lee, T. S.; Kim, J. *Adv. Mater.* **2008**, *20*, 1117.
(11) (a) Becker, W. G.; Bard, A. J. *J. Phys. Chem.* **1983**, *87*, 4888. (b) Van Dijken, A.; Meulenkamp, E. A.; Vanmaekelbergh, D.; Meijerink, A. *J. Phys. Chem. B* **2000**, *104*, 1715.
(12) Deniz, A. A.; Laurence, T. A.; Dahan, M.; Chemla, D. S.; Schultz, P. G.; Weiss, S. *Annu. Rev. Phys. Chem.* **2001**, *52*, 233.
(13) Wu, C. L.; Zheng, J. S.; Huang, C. B.; Lai, J. P.; Li, S. Y.; Chen, C.; Zhao, Y. B. *Angew. Chem., Int. Ed.* **2007**, *46*, 5393.
(14) (a) Becker, W. G.; Bard, A. J. *J. Phys. Chem.* **1983**, *87*, 4888. (b) Van Dijken, A.; Meulenkamp, E. A.; Vanmaekelbergh, D.; Meijerink, A. *J. Phys. Chem. B* **2000**, *104*, 1715. (c) Norberg, N. S.; Gamelin, D. R. *J. Phys. Chem. B* **2005**, *109*, 20810.
(15) (a) Shen, G. Z.; Chen, D.; Lee, C. J. *J. Phys. Chem. B* **2006**, *110*, 15689. (b) Joo, J.; Na, H. B.; Yu, T.; Yu, J. H.; Kim, Y. W.; Wu, F. X.; Zhang, J. Z.; Hyeon, T. *J. Am. Chem. Soc.* **2003**, *125*, 11100. (c) Du, J. M.; Fu, L.; Liu, Z. M.; Han, B. X.; Li, Z. H.; Liu, Y. Q.; Sun, Z. Y.; Zhu, D. B. *J. Phys. Chem. B* **2005**, *109*, 12772.
(16) (a) Bagnall, D. M.; Chen, Y. F.; Zhu, Z.; Yao, T.; Koyama, S.; Shen, M. Y.; Goto, T. *Appl. Phys. Lett.* **1997**, *70*, 2230. (b) Huang, M. H.; Mao, S.; Feick, H.; Yan, H. Q.; Wu, Y. Y.; Kind, H.; Weber, E.; Russo, R.; Yang, P. D. *Science* **2001**, *292*, 1897. (c) Guo, L.; Ji, Y. L.; Xu, H. B.; Wu, Z. Y.; Simon, P.; Wu, Z. Y. *J. Am. Chem. Soc.* **2002**, *124*, 14864.
(17) Chen, Y. F.; Rosenzweig, Z. *Anal. Chem.* **2002**, *74*, 5132.
(18) Costa-FernOndez, J. M.; Pereiro, R.; Sanz-Medel, A. *TrAC Trends Anal. Chem.* **2006**, *25*, 207.
(19) Liang, J. G.; Ai, X. P.; He, Z. K.; Pang, D. W. *Analyst* **2004**, *129*, 619.
(20) Dong, C.; Qian, H.; Fang, N.; Ren, J. *J. Phys. Chem. B* **2006**, *110*, 11069.
(21) Ali, E. M.; Zheng, Y. G.; Yu, H. H.; Ying, J. Y. *Anal. Chem.* **2007**, *79*, 9452.
(22) Xia, Y. S.; Zhu, C. Q. *Talanta* **2008**, *75*, 215.

the UV emission band contributed by ZnO NRs shows a constant intensity in all cases since the surface of the NRs was absent of functional groups to interact with these ions, which makes the mesoporous CdTe/ZnO@SiO_2 nanostructures be ideal fluorescence sensing materials.

Experimental Section

Materials. Zinc acetate, potassium hydroxide, sodium hydroxide, cadmium chloride, tellurium powders (99.99%), sodium borohydride ($NaBH_4$), cetyltrimethylammonium bromide (CTAB) and methanol are all analytical grade (Shanghai Chemical Reagents Co.) and used without further purification. Thioglycollic acid (TGA) and tetraethyl orthosilicate (TEOS) were purchased from Alfa Aesar.

Synthesis of Colloidal ZnO NRs.[23] In a typical process, 14.75 g of zinc acetate was dissolved in 60 mL of methanol, and the solution was refluxed at 65 °C until all solids were dissolved. In addition, 7.4 g of potassium hydroxide was dissolved with 32 mL of methanol at room temperature. Then, the solution containing potassium hydroxide was poured into the zinc acetate solution under vigorous stirring. It was observed that white colloids were formed immediately. The colloids must be ripened at 65 °C for at least three days in order to get NRs with a narrow size distribution and to perfect their surface structures. After that, ZnO NRs were separated from the solution by centrifugation at 2000 rpm, washed repetitively with distilled water, and dried at 40 °C under vacuum.

Synthesis of TGA-Stabilized CdTe QDs.[24] A total of 0.228 g cadmium chloride ($CdCl_2 \cdot 2.5H_2O$) and 0.11 g of TGA were dissolved in 50 mL distilled water, and the pH of the solution was adjusted to pH 9.0 with 1 M sodium hydroxide solution. The mixture was then deaerated by bubbling nitrogen for 30 min. Under stirring, a certain volume of fresh oxygen-free NaHTe solution, prepared by the reaction of tellurium powder with $NaBH_4$, was injected rapidly into the reaction mixture. After that, the mixture was refluxed; the particle size of the QDs was controlled by the reflux time. Solid CdTe QDs were precipitated by the addition of absolute ethanol to the as-prepared solution. The resulting precipitate was centrifuged, washed with ethanol, and dried in a desiccator before use. Typically, CdTe QDs synthesized via the present aqueous route is cubic in structure (JCPDS file, No.75-2086).[25]

Synthesis of Mesoporous CdTe/ZnO@SiO_2 Core/Shell Nanostructures. In a typical process, 50 mL of absolute alcohol, 1 mL of distilled water, 1.7 mL of aqueous ammonia, and 200 μL of TEOS were injected into a 100 mL conical flask; this solution was stirred for 10 min at 40 °C. After that, CdTe QDs (0.008 g), ZnO NRs (0.035 g), and CTAB (0.1 g) dispersed ultrasonically in distilled water (10 mL) were added to the foregoing solution. The mixture was continuously stirred for 12 h at 40 °C. The resulting ternary nanocomposites consisting of SiO_2 shell, ZnO NRs, and CdTe QDs were then isolated by centrifugation and washed with hot deionized water to remove excess QDs as well as CTAB as much as possible, which could avoid the adverse effects of CTAB on the surface area and PL property of the product. For each washing, the sonicator was used to completely disperse the nanoparticles in water.

Fluorescence Response of Mesoporous CdTe/ZnO@SiO_2 Core/Shell Nanostructures to Hg^{2+}, Pb^{2+}, and Cu^{2+}. At first, 0.05 g of CdTe/ZnO@SiO_2 nanocomposites were dispersed in 20 mL of absolute alcohol to form a stable colloidal solution. Different amounts ($10^{-5}-10^{-9}$ M) of Cu^{2+}, Hg^{2+}, and Pb^{2+} ions in absolute alcohol were also prepared. Then, 250 μL of the CdTe/ZnO@SiO_2 dispersion was injected to a clean volumetric flask and diluted to 10 mL with the above solution of Cu^{2+}, Hg^{2+}, or Pb^{2+} ions. The resulting mixtures were incubated for 12 h at room temperature. After that, an Edinburgh FLS-920 Steady-State/Lifetime spectrofluorometer was applied to record their fluorescence spectra. All samples were excited under a same wavelength of 330 nm.

Characterization of Products. The powder X-ray diffraction (XRD) patterns of the samples were recorded by an X'Pert PRO SUPER rA rotation anode X-ray diffractometer with Ni-filtered Cu Kα radiation ($\lambda = 1.54178$ Å). The X-ray photoelectron spectroscopy (XPS) measurements were performed on a Vgescalab MK II X-ray photoelectron spectrometer (XPS) using Mg Kα radiation ($h\nu = 1253.6$ eV) with a resolution of 1.0 eV. The microstructures and morphologies of the products were investigated by a FEI Tecnai G20 transmission electron microscope (TEM) and a Hitachi S-4700 field emitting scanning electron microscope (FESEM). High-resolution transmission electron microscopy (HRTEM) images of the products were taken at 200 kV with a JEOL-2010 TEM. Energy-dispersive X-ray (EDS) measurements were performed with the spectrometer attached on the JEOL-2010 TEM. The nitrogen adsorption−desorption isotherms, BET surface, and pore-size distribution were measured on a Micromeritics ASAP 2020 instrument. The UV−vis absorption spectra of the products were measured on a Shimadzu 3150 UV−vis−near-infrared spectrophotometer. Room-temperature PL spectra were performed on an Edinburgh FLS-920 Steady-State/Lifetime spectrofluorometer under an excitation wavelength of 330 nm. The samples for optical absorption and PL measurements were prepared by dispersing the solid products into absolute alcohol.

Results and Discussion

Structure and Morphology of Mesoporous CdTe/ZnO@SiO_2 Core/Shell Nanostructures. Figure 1 shows the structure and morphology characterization of the initial ZnO NRs for preparing the core−shell nanocomposites. As seen from TEM image (Figure 1a) and FESEM image (Figure 1b), the product is composed of monodispersed NRs with an extremely high yield. The mean dimensions of the nanorods are length, 84.7 ± 3.8 nm; diameter, 11.9 ± 1.5 nm, which were extracted from the TEM images of 300 nanorods (the size dispersity of the nanorods was shown in Supporting Information). Figure 1c was a representative HRTEM image of the NRs; the well-resolved lattice fringes demonstrate that the NRs are highly crystalline. The interplanar spacing of 2.62 Å is close to the separation between the (002) crystallographic planes of hexagonal ZnO. The nanorods were grown preferentially along the common [001] direction. In addition, the surfaces of these ZnO NRs are surrounded by large amounts of hydroxyl groups,[23b] which is advantageous to the dispersion of them into water or alcohol to form stable colloids. Consequently, these monodispersed, water-soluble ZnO NRs are ideal building blocks in the fabrication of various functional nanocomposites.

Figure 2 displays the XRD pattern of the as-prepared CdTe/ZnO@SiO_2 core/shell nanostructures, and for a comparison, the XRD pattern of the initial ZnO NRs is also

(23) (a) Pacholski, C.; Kornowski, A.; Weller, H. *Angew. Chem., Int. Ed.* **2002**, *41*, 1188. (b) Guo, Y.; Cao, X. B.; Lan, X. M.; Zhao, C.; Xue, X. D.; Song, Y. Y. *J. Phys. Chem. C* **2008**, *112*, 8832.
(24) (a) Gaponik, N.; Talapin, D. V.; Rogach, A. L.; Hoppe, K.; Shevchenko, E. V.; Kornowski, A.; EychMüller, A.; Weller, H. *J. Phys. Chem. B* **2002**, *106*, 7177. (b) Bao, H.; Gong, Y.; Li, Z.; Gao, M. *Chem. Mater.* **2004**, *16*, 3853. (c) Guo, J.; Yang, W. L.; Wang, C. C. *J. Phys. Chem. B* **2005**, *109*, 17467.
(25) Cao, X. B.; Lan, X. M.; Guo, Y.; Zhao, C. *Cryst. Growth Des.* **2008**, *8*, 575.

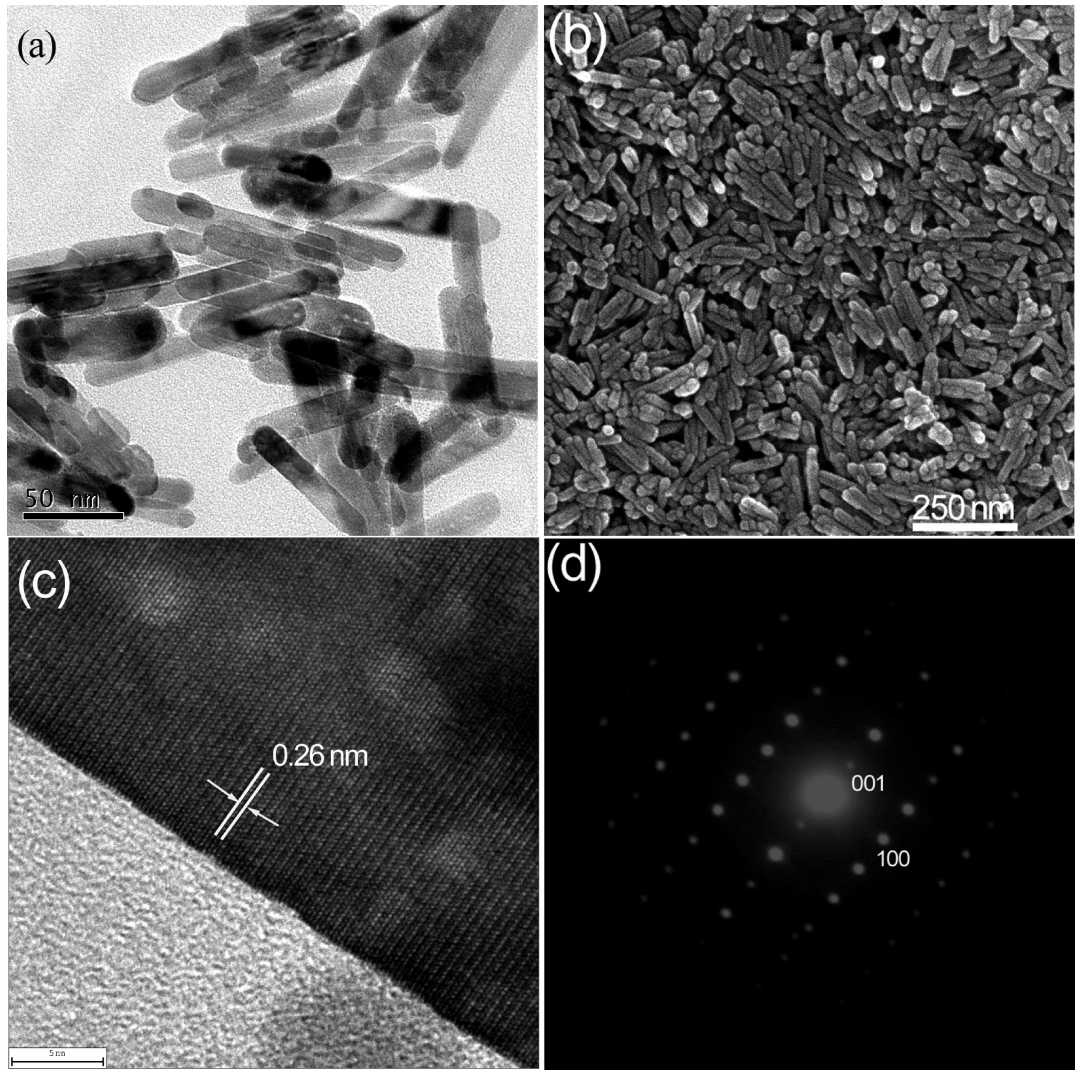

Figure 1. (a) TEM image of ZnO NRs. (b) FESEM image of ZnO NRs. (c) HRTEM image of ZnO NRs. (d) A typical SAED pattern.

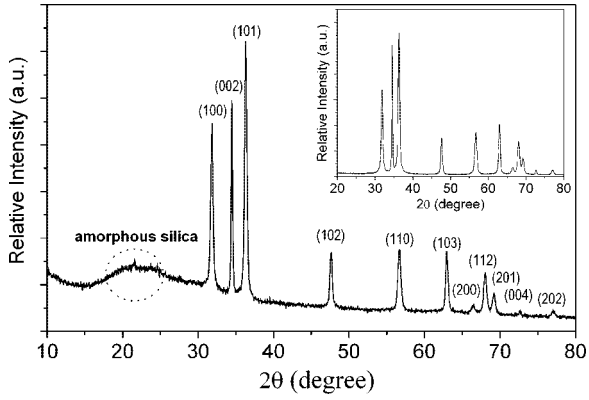

Figure 2. XRD pattern of CdTe/ZnO@SiO$_2$ core/shell nanostructures. For a comparison, the XRD pattern of ZnO NRs was included (inset).

shown (the inset in Figure 2). The broad peak around 23° in the nanocomposites is typically caused by amorphous silica, and accordingly this result indicates the existence of the component of SiO_2. Except the broad peak around 23°, all the other peaks in the figure can be attributed to hexagonal wurtzite ZnO.[26] But the reflections corresponding to CdTe QDs were not detected, which should be related to the poor crystallinity of CdTe QDs, the low content of CdTe QDs in the nanocomposites, and the shielding of the signals by the wide peak of amorphous silica (the strongest XRD peak of cubic CdTe is around 24°).[25]

XPS is a sensitive tool for the analysis of the surface chemical compositions of materials, and hence, XPS spectra of the as-prepared nanocomposites were recorded in order to gain more structure information of them. Figure 3 was the typical XPS spectra of the nanocomposites with a reacting time of 12 h, where part a was the survey spectrum and parts b−d were the high-resolution binding energy spectra for Cd, Zn, and Si species, respectively. According to the survey spectrum, the elements of Zn, Si, Cd, Te, O, and S were found, of which the elements of Zn, Si, and O arise from the components of ZnO NRs and SiO_2, the elements of Te and Cd arise from CdTe QDs, and the element of S arises from TGA molecules capped on the surfaces of CdTe QDs. These results indicate that the nanocomposites are composed of three components, ZnO, CdTe, and SiO_2. Table 1 listed the values of binding energy of Zn, Cd, and Si resolved from XPS spectra of the nanocomposites with reacting times of 3 and 12 h. In both cases, the values of binding energy of Cd $3d^5$, Zn $2p^3$, and Si 2p were very close. Relative to

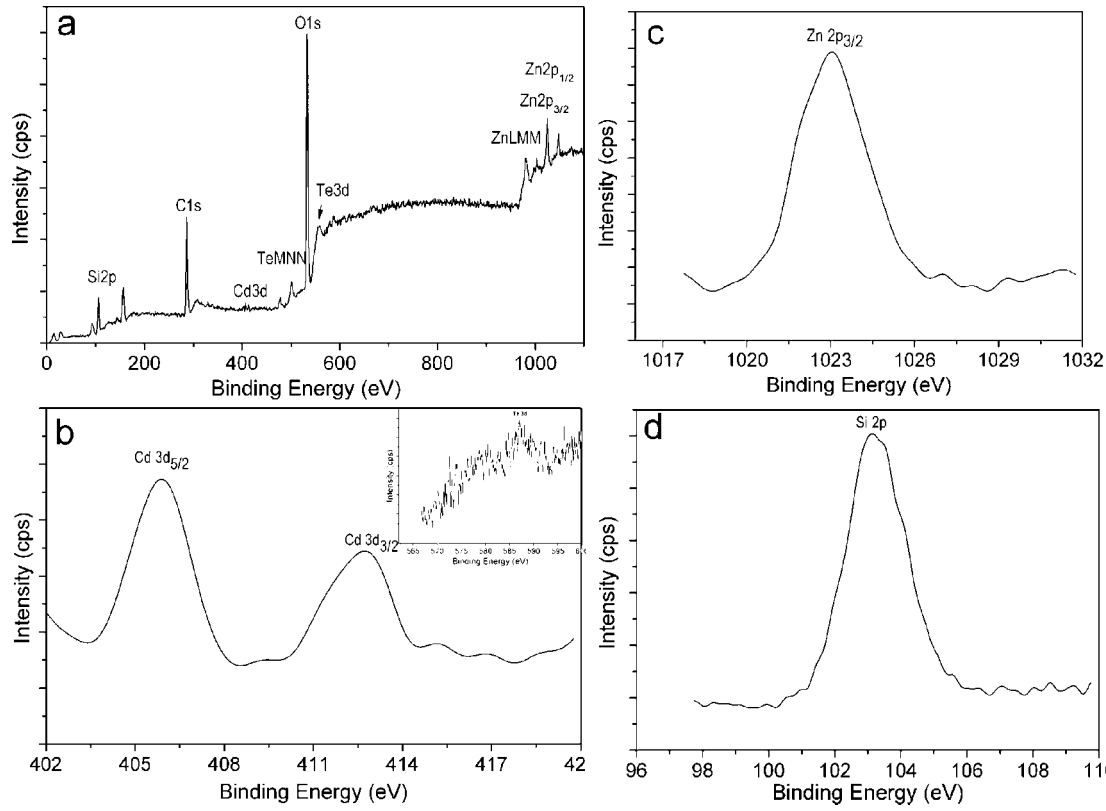

Figure 3. XPS spectra of CdTe/ZnO@SiO_2 core/shell nanostructures. (a) XPS survey spectrum. (b) Binding energy spectrum of Cd 3d. Inset: binding energy spectrum of Te 3d. (c) Binding energy spectrum of Zn 2p. (d) Binding energy spectrum of Si 2p.

Table 1. Standard Binding Energy Values for Zn 2p, Cd 3d, and Si 2p and Those Resolved in CdTe/ZnO@SiO_2 Core/Shell Nanostructures[27a]

	Zn $2p^3$	Cd $3d^5$	Si 2p
binding energy in the nanocomposites (reacting time: 3 h)	1022.99	405.78	103.15
binding energy in the nanocomposites (reacting time: 12 h)	1023.02	405.81	103.13
standard value	1022.50	404.90	103.43

[a] Unit for binding energy: eV.

the standard values,[27] there is an increase for the values of binding energy of Cd $3d^5$ and Zn $2p^3$ but a slight decrease for the value of binding energy of Si 2p. So, interactions should exist among ZnO NRs, CdTe QDs, and SiO_2 and cause the change of binding energies of Cd, Zn, and Si. That is, it may deduce that ZnO NRs and CdTe QDs have been confined into one common nanostructure by SiO_2, thereby leading to the interactions to certain extent among them.

Figure 4 displays the TEM, FESEM, and HRTEM images of CdTe/ZnO@SiO_2 core/shell nanostructures. Parts a and c of Figure 4 correspond to the product that is prepared by reacting TEOS with ZnO NRs and CdTe QDs for 3 h, while parts b and d of Figure 4 correspond to the product with a reacting time of 12 h. As seen from TEM images (Figure 4a,b), ZnO NRs were embedded within SiO_2 matrix, and thereby the products possess a distinct core−shell-like structure, which confirm our presumption based on the results of XPS measurements. Since the sizes of CdTe QDs were too small, it is rather difficult to distinguish them from the SiO_2 matrix. For the nanocomposite with a reacting time of 3 h, the average thickness of the SiO_2 shell is about 4 nm, whereas the thickness of the SiO_2 shell is increased to 8 nm when the reacting time reaches 12 h. That is, the thickness of the SiO_2 shell can be adjusted by regulating the reacting time. The results of FESEM (Figure 4c,d) observations of the products are consistent with TEM; they clearly exhibit that the products are worm-like shapes after the encapsulation of SiO_2, which is totally different from the short and straight feature of ZnO NRs. Figure 4e shows a HRTEM image of the CdTe/ZnO@SiO_2 nanocomposites with a reacting time of 12 h, which provides further evidence to prove the well-defined core/shell feature of the nanocomposites. In addition, it is seen that CdTe QDs were mainly adsorbed on the surface of ZnO NRs, as indicated by arrows in Figure 4e. This result is understandable. Since the surfaces of TGA-stabilized CdTe QDs are rich of carboxyl groups with good affinity to metal ions, CdTe QDs have a strong tendency to chemically link onto the surfaces of ZnO NRs. Obviously, the adsorption of QDs increase the diameters of ZnO NRs, and hence, ZnO NRs within the nanocomposites seem to have a relatively larger diameter than those uncoated with silica shell. Figure 4f displays the associated EDS spectrum of the CdTe/ZnO@SiO_2 nanocomposites, which reveals the existence of CdTe QDs in the nanocomposites too. According to EDS analysis, the weight content (wt %) of CdTe QDs in the core/shell nanostructures with a reacting time of 3 and 12 h was found to be 2.2% and 5.9%, respectively, whereas that of ZnO NRs in both cases was

(26) Joint Committee on Powder Diffraction Standards, JCPDS file No. 80-0075.
(27) Wagner, C. D.; Riggs, W. W.; Davis, L. E.; Moulder, J. F.; Muilenberg, G. E. *Handbook of X-Ray Photoelectron Spectroscopy*; Perkin-Elmer Corporation, Physical Electronics Division, 1979.

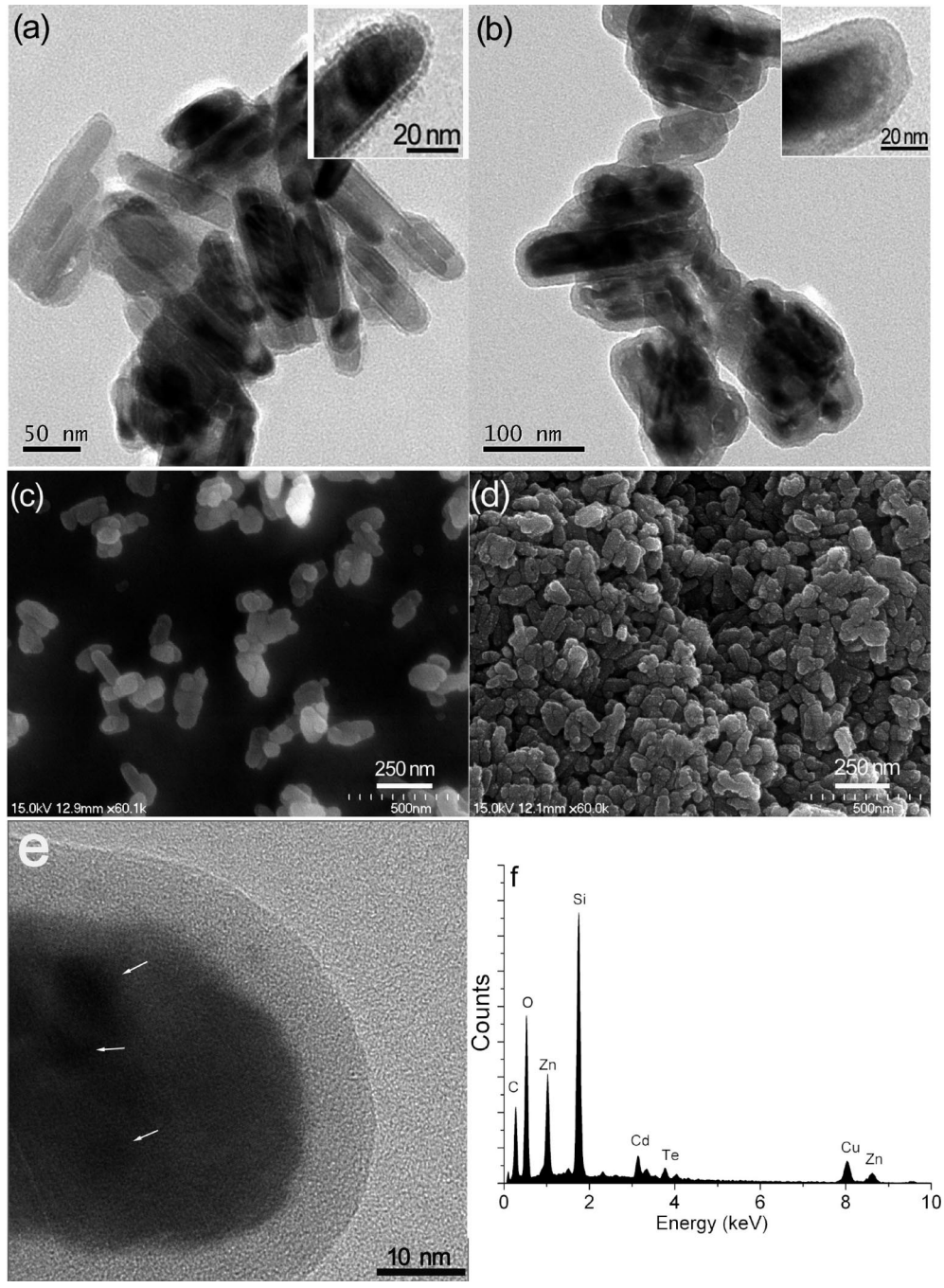

Figure 4. (a, c) TEM and FESEM images of CdTe/ZnO@SiO_2 core/shell nanostructures (reacting time: 3 h). (b, d) TEM and FESEM images of CdTe/ZnO@SiO_2 core/shell nanostructures (reacting time: 12 h). The insets in parts a and b exhibited an individual core/shell nanostructure. (e) HRTEM image taken on an individual core−shell structure, where the arrows indicate the QDs attached. (f) EDS spectrum of CdTe/ZnO@SiO_2 core/shell nanostructures.

very close (27.0% vs 28.1%). It is because only parts of QDs were encapsulated by the silica shell at the early stage of hydrolysis of TEOS, while other QDs still remained in the solution due to their good solubility and stability. In experiments it can be clearly seen that, after solid product was separated from the solution by centrifugation, the supernatant possessed the characteristic color of QDs at this stage. With the increase of the hydrolysis time of TEOS, the silica shell became thick and more QDs would be encapsulated. So, the content of QDs in the nanocomposites with hydrolysis time of 3 and 12 h was largely different.

The N_2 adsorption/desorption isotherms (Figure 5a) of CdTe/ZnO@SiO_2 core/shell nanostructures exhibited a type IV isotherm with a hysteresis loop, demonstrating the mesoporous characteristics of the silica shell. In addition, small-angle X-ray scattering (SAXS) measurements also reveal that the silica shell was mesoporous (Supporting Information). Calculated from the desorption branch of the nitrogen isotherm with the BJH method, an average pore diameter is determined to be 4.1 nm. The BET surface area and the BJH desorption cumulative volume of pores of the nanocomposites are 254.7 m^2/g and 0.253 cm^3/g, respectively, which are considerably large since ZnO NRs and CdTe QDs have been included in the calculations. Besides N_2 adsorption/desorption, the results of small-angle X-ray scattering (SAXS) also revealed that CdTe/ZnO@SiO_2 core/

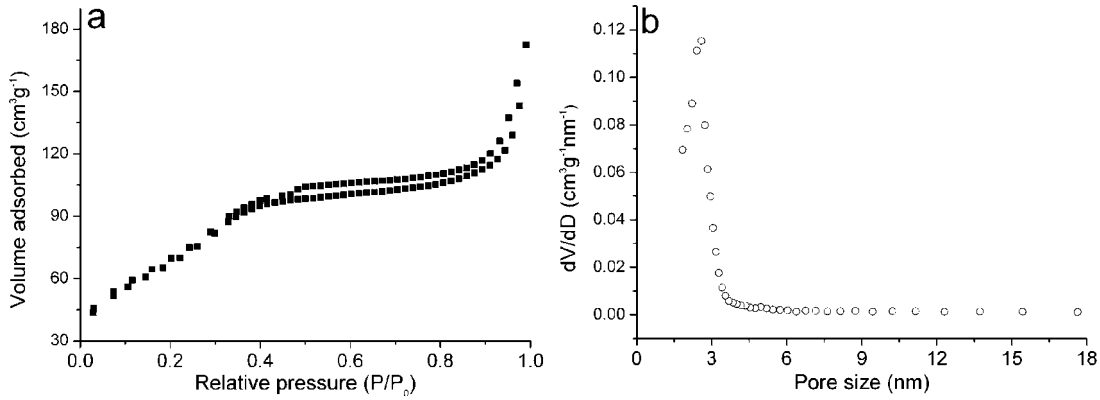

Figure 5. (a) N_2 adsorption/desorption isotherms. (b) Corresponding pore size distribution curve from desorption branch.

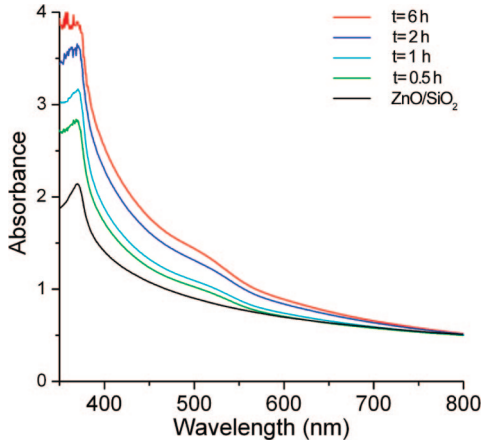

Figure 6. UV−vis absorption spectra of CdTe/ZnO@SiO_2 core/shell nanostructures with different reacting time (color lines) and ZnO@SiO_2 nanocomposites (black line).

shell nanostructures were mesoporous. The mesoporosity should be a preferable property of CdTe/ZnO@SiO_2 core/shell nanostructures if they are applied in florescence sensing, which is because the pores allow the entering of molecules and ions to contact with QDs and result in an enhanced adsorption of these objects.

Optical Properties of CdTe/ZnO@SiO_2 Core/shell Nanostructures. In this study, the optical properties of CdTe/ZnO@SiO_2 nanocomposites were characterized by UV−visible absorption and PL spectroscopy, respectively. Figure 6 shows the absorption spectra (colored lines) of the nanocomposites with different reacting times. For a comparison, the absorption spectrum of the nanocomposites containing only ZnO NRs was also included (black curve in Figure 6). In all these samples, the prominent band centered at 372 nm is known to originate from the band-edge absorption of ZnO NRs. For ZnO@SiO_2 nanocomposites, the absorption curve is smooth in the region of visible light. For CdTe/ZnO@SiO_2 nanocomposites, a narrow absorption band around 550 nm arises, which is a typical optical feature of CdTe QDs. And as the prolongation of the hydrolysis time of TEOS, the intensity of the visible absorption band is gradually enhanced, which means that the amount of CdTe QDs encapsulated is increased. EDS analysis revealed that the content of QDs (wt %) at the stage of 0.5 h, 1 h, 2 h, and 6 h is 0.6%, 1.1%, 1.8%, and 4.3%, respectively. Consequently, the content of CdTe QDs within the core/shell nanostructures can be controlled by regulating the hydrolysis time of TEOS. The ability to control the amount of QDs in the nanocomposites is very important because it directly determines the optical properties of the nanostructures (e.g., absorption and PL intensity).

Figure 7 shows the room temperature PL spectra of the nanocomposites. If the nanocomposites contain only ZnO NRs, they feature a narrow UV emission band centered at 373 nm, which can be assigned to excitonic recombination in ZnO (black line in Figure 7a). But for CdTe/ZnO@SiO_2 core/shell nanostructures, additional visible emission band contributed by CdTe QDs appears (color lines in Figure 7a), which means that CdTe/ZnO@SiO_2 nanocomposites possess simultaneously UV and visible fluorescence. The position of the visible emission band was tuned by introducing different colors of QDs into the nanostructures. Herein we have prepared three core/shell nanostructures with visible emission band centered at 515 nm, 539 nm, and 582 nm, respectively (Figure 7a). Besides the ability to control the wavelength of visible emission, it is also possible to regulate the fluorescence intensity ratio of the dual emission in the CdTe/ZnO@SiO_2 nanocomposites. Considering that the intensity ratio of the dual emission is dependent on the relative content of ZnO NRs and CdTe QDs in the nanocomposites, we have adjusted the hydrolysis time of TEOS to realize the control of it. For example, if the hydrolysis time of TEOS was shorter than 1 h, the prominent fluorescence of the ternary nanocomposites comes from the UV emission of ZnO NRs (Figure 7b). With the prolongation of the hydrolysis time of TEOS that will increase the thickness of the SiO_2 shell and the content of CdTe QDs encapsulated, visible emission from QDs instead of UV emission serves as the prominent fluorescence of the nanocomposites (Figure 7b). Its intensity keeps constant after the hydrolysis time reaches 12 h. In a word, the above results demonstrate that as-prepared CdTe/ZnO@SiO_2 nanocomposites are bilumiscent nanomaterials with controllable visible emission.

Ultrasensitive Fluorescence Response of CdTe/ZnO@SiO_2 Core/Shell Nanostructures to Cu^{2+}, Hg^{2+}, and Pb^{2+} Ions. The fluorescence properties of Cd chalcogenide QDs are closely related to the nature of their surface.[28] The interactions of QDs with heavy-metal ions, small molecules, or biomacromolecules will cause the modification of the surface of QDs, and as a result, the fluorescence intensity of QDs was enhanced or quenched. In return, the

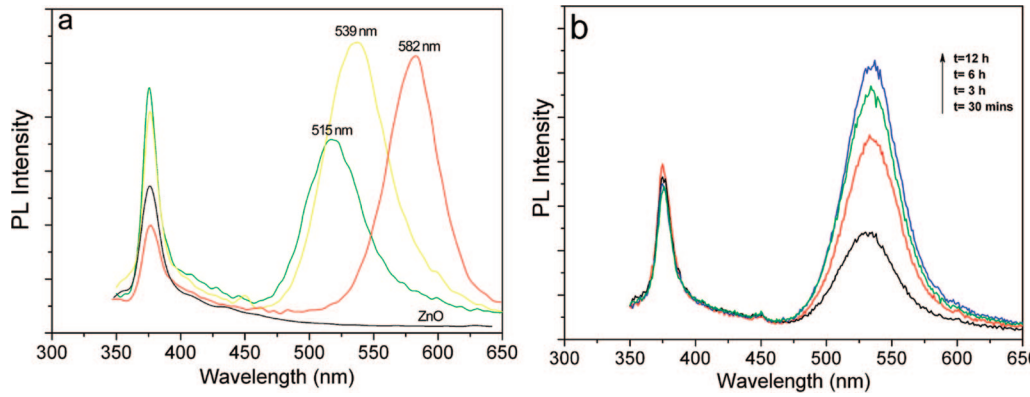

Figure 7. (a) Room-temperature PL spectra of ZnO@SiO$_2$ nanocomposites (black line) and CdTe/ZnO@SiO$_2$ core/shell nanostructures with a visible-emission band centered at 515 nm, 539 nm, and 582 nm (color lines). (b) Room-temperature PL spectra of CdTe/ZnO@SiO$_2$ nanocomposites with a reacting time of 30 min, 3 h, 6 h, and 12 h.

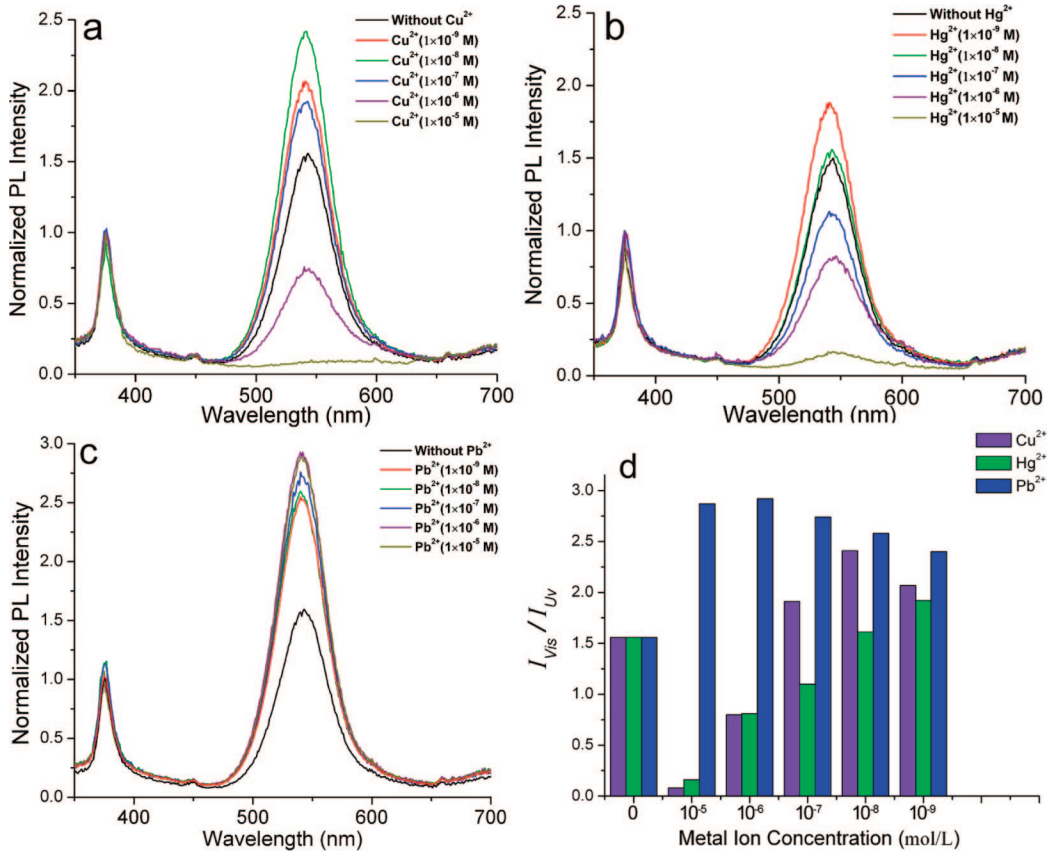

Figure 8. Normalized PL spectra of CdTe/ZnO@SiO$_2$ core/shell nanostructures incubated with different amounts of Cu^{2+} (a), Hg^{2+} (b), and Pb^{2+} (c). The incubation time is 12 h. (d) Correlations between the metal ion concentration and the fluorescence intensity ratio of the dual emission in the nanocomposites.

change of the fluorescence intensity of QDs can serve as a parameter to indicate the content of heavy-metal ions, small molecules, and biomacromolecules.[17−22] Since herein fluorescent CdTe/ZnO@SiO$_2$ nanocomposites were water soluble and possess a mesoporous surface, they should be particularly suitable for fluorescence sensing materials. On the basis of this principle, we have investigated the interactions of the nanocomposites with heavy-metal ions of Cu^{2+}, Hg^{2+}, and Pb^{2+} and the associated PL behaviors. Figure 8a−c displays the representative PL spectra of the nanocomposites incubated with different amounts of Cu^{2+}, Hg^{2+}, and Pb^{2+} ions for 12 h. In all cases, the intensities of UV emission were almost invariable by the addition of metal ions, while the visible emission contributed by QDs was enhanced or quenched, dependent on the concentration of the metal ions. Such PL behaviors demonstrate that Cu^{2+}, Hg^{2+}, or Pb^{2+} ions interact strongly with CdTe QDs, thereby causing the change of the surface properties and the fluorescence intensity of the QDs. In contrast, the surface of ZnO NRs was short of functional groups to interact with the metal ions, and therefore, the fluorescence intensity of UV emission of the nanocomposites was not influenced. By the way, the variable visible emission vs the constant UV emission means that one can use the fluorescence intensity ratio of the dual

emission to indicate the amount of the metal ions, which will be more reliable and precise than the common single-signal fluorescence probes.

At a relatively high Cu^{2+} and Hg^{2+} concentration (10^{-5} M and 10^{-6} M for Cu^{2+} ions and $10^{-5}-10^{-7}$ M for Hg^{2+} ions), the intensity of the visible emission was reduced (parts a and b of Figure 8). It is very interesting that, when a lower concentration of Cu^{2+} and Hg^{2+} ions was used, the fluorescence intensity of QDs was enhanced instead. The enhancement amplitude can reach 62% at $M_{Cu^{2+}} = 10^{-8}$ M and 31% at $M_{Hg^{2+}} = 10^{-9}$ M, relative to the fluorescence intensity of the nanocomposites without interactions with the metal ions. For Pb^{2+} ions, they always result in the enhancement of the intensity of the visible emissions below a concentration of 10^{-5} M (part c of Figure 8). The maximum fluorescence enhancement (~93%) appears at $M_{Pb^{2+}} = 10^{-6}$ M. It should be noted that the abnormal fluorescence enhancement can be excluded to be caused by errors or other uncertain factors, as learned from the constant UV emission intensity. Additionally, to determine whether the fluorescence behaviors have batch to batch reproducibility or not, at least four groups of parallel experiments were conducted. The results show that the change of the fluorescence intensities has a similar tendency in these experiments. Figure 8d plots the correlations between the concentrations of Cu^{2+}, Hg^{2+}, and Pb^{2+} ions and the intensity ratio of the dual emission, which are the average results of four parallel experiments.

Previously, it is generally accepted that heavy metal ions are effective quenchers of the fluorescence of QDs. Only a few reports pointed out that the fluorescence of QDs was enhanced upon the addition of Cd^{2+},[29] Mn^{2+},[30] Zn^{2+},[17,29,31] and Ag^{+}.[32] The mechanism accounting for the fluorescence quenching of QDs was thought to be the displacement of Cd by heavy metal ions or the coordination between heavy metal ions and the surface functional groups (e.g., carboxyl) of the QDs. Upon metal ion displacement, the nonradiative electron/hole recombination annihilation will be facilitated, and the feature of this quenching process is the red or blue shift of the absorption and emission spectra of the QDs, as reported by Chrysochoos's[33] and Ren's groups.[20] If metal ions were coordinated with the capping agents on the surface of QDs, surface ligand stripping and the aggregation of the QDs would occur, causing the fluorescence quenching of QDs. Recently, Ying's group reported that QDs capped with glutathione began to aggregate at Pb^{2+} concentration higher than 0.25 mM.[21]

In contrast, we found that low concentrations of Cu^{2+}, Hg^{2+}, and Pb^{2+} ions were all capable of enhancing the visible emission contributed by CdTe QDs in the nanocomposites, and the emission band was fixed at 539 nm in all cases (Figure 8). In addition, the aggregation phenomenon was not observed even if the nanocomposites were incubated with Cu^{2+}, Hg^{2+}, and Pb^{2+} ions with a concentration as high as 1 mM. Consequently, the surface properties of the CdTe QDs within the core−shell CdTe/ZnO@SiO_2 nanocomposites were quite different from those in previous reports. We believe the difference arises from the encapsulation of mesoporous silica shell on the surface of the QDs, whereas the QDs in previous reports were only capped by small organic ligands. The silanization of the surface of semiconductors has shown great success in protecting their surface characteristics, which prevents flocculation of particles and helps to maintain the photoluminescence.[34] In our work, the mesoporous silica shell of CdTe/ZnO@SiO_2 nanostructures plays multiple roles. In the first, the pores allow Cu^{2+}, Hg^{2+}, and Pb^{2+} ions to enter into the interior of the nanostructures to contact with QDs, accordingly causing a fluorescence response. Second, the silica layer on the surface of QDs may effectively prevent the binding of Cu^{2+}, Hg^{2+}, and Pb^{2+} ions with the QDs core and avoid the displacement of Cd atoms. This presumption is supported by the fixed visible-emission band at 539 nm whether the nanocomposites were incubated with the metal ions or not (parts a−c of Figure 8). Third, the QDs were anchored tightly on the surface of ZnO NRs and separated from each other by the silica layer. Consequently, the coordination of high-concentration Cu^{2+}, Hg^{2+}, and Pb^{2+} ions with the surface carboxyl of TGA-capped QDs did not cause the aggregation or precipitation of them. Finally, the mesoporous property of the core−shell CdTe/ZnO@SiO_2 nanocomposites results in the enhanced adsorption of metal ions. Even if they were incubated with trace Cu^{2+}, Hg^{2+}, and Pb^{2+} ions, obvious fluorescence response was still observed. An analogous result was reported by Kotov's group,[28b] who found that silica-coated QDs were photoactivated more easily than naked QDs due to the enchantment adsorption of the oxygen available for eliminating the surface defects of QDs. Herein, TGA-capped CdTe QDs were synthesized in aqueous media at low temperature, and therefore there are certain trap sites on the QDs surface. Under appropriate concentrations, the adsorbed Cu^{2+}, Hg^{2+}, and Pb^{2+} ions on the trap sites may help to passivate the QDs surface and cause the fluorescence enhancement.[20,29,32] When the initial traps were saturated, the excess metal ions would facilitate nonradiative electron/hole recombination annihilation through an effective electron transfer process between capping ligands and the metal ions. Consequently, there exists an optimal ion concentration to increase the fluorescence of the nanocomposites. As seen from Figure 8, such a concentration for Cu^{2+}, Hg^{2+}, and Pb^{2+} ions was 10^{-8} M, 10^{-9} M, and 10^{-6} M, respectively.

Conclusions

In summary, CdTe QDs and ZnO NRs were encapsulated by a layer of mesoporous SiO_2 to form CdTe/ZnO@SiO_2

(28) (a) Woggon, U. *Optical Properties of Semiconductor Quantum Dots*; Springer: Berlin, Germany, 1997. (b) Wang, Y.; Tang, Z. Y.; Correa-Duarte, M.; Pastoriza-Santos, I.; Giersig, M.; Kotov, N.; Liz-Marzàn, L. *J. Phys. Chem. B* **2004**, *108*, 15461. (c) Myung, N.; Bae, Y.; Bard, A. J. *Nano Lett.* **2003**, *3*, 747. (d) Reiss, P.; Bleuse, J.; Pron, A. *Nano Lett.* **2002**, *2*, 781.
(29) Moore, D. E.; Patel, K. *Langmuir* **2001**, *17*, 2541.
(30) Sooklal, K.; Cullum, B. S.; Angel, S. M.; Murphy, C. J. *J. Phys. Chem.* **1996**, *100*, 4551.
(31) Li, J.; Bao, D. S.; Hong, X.; Li, D.; Li, J. H.; Bai, Y. B.; Li, T. J. *Colloids Surf., A* **2005**, *257*, 267.
(32) Xia, Y. S.; Cao, C.; Zhou, C. Q. *J. Lumin.* **2008**, *128*, 166.
(33) Isarov, A. V.; Chrysochoos, J. *Langmuir* **1997**, *13*, 3142.
(34) Wolcott, A.; Gerion, D.; Visconte, M.; Sun, J.; Schwartzberg, A.; Chen, S. W.; Zhang, J. Z. *J. Phys. Chem. B* **2006**, *110*, 5779.

core/shell nanostructures. Due to the contributions of visible emission by QDs and ultraviolet emission by NRs, the core/shell nanostructures are biluminescent in nature. The fluorescence intensity ratio of the dual emission can be tuned by regulating the hydrolysis time of TEOS. The wavelength of the visible emission was also tunable in a wide range by altering the size of QDs introduced. Interestingly, the core−shell CdTe/ZnO@SiO_2 nanocomposites exhibit ultrasensitive fluorescence response to Hg^{2+}, Pb^{2+}, and Cu^{2+} ions. Trace Cu^{2+} ($\leq 10^{-7}$ M), Hg^{2+} ($\leq 10^{-7}$ M), and Pb^{2+} ($\leq 10^{-5}$ M) could enhance the visible emission in the nanocomposites, which is quite different from the fluorescence quenching effect of these heavy-metal ions in previous reports. The fluorescence enhancement is presumed to be the results of the adsorption of the metal ions on the trap sites of QDs surface and the passivation of the QDs. The mesoporous silica shell of the nanocomposites also plays key roles in the process of fluorescence enhancement, which protects the surface characteristics of QDs, prevents the flocculation of the particles, and promotes the adsorption of Cu^{2+}, Hg^{2+}, and Pb^{2+} ions. Unlike the variable fluorescence of QDs, the intensity of the UV emission band is not affected due to the inert surface of ZnO NRs, which will favor more reliable fluorescence sensing. Consequently, the CdTe/ZnO@SiO_2 core/shell nanostructures are ideal biluminescent materials and ultrasensitive ion probes. We also believe that they should be also powerful in the fluorescence detection of biomolecules, and it is under investigations now.

Acknowledgment. This work was financially supported by National Natural Science Foundation of China (20601020), Key Laboratory of Organic Synthesis of Jiangsu Province (China), and National Natural Science Foundation of Zhejiang Province (China).

Supporting Information Available: Size dispersity of ZnO nanorods, TEM images, absorption and PL spectra of various CdTe QDs for preparing CdTe/ZnO@SiO_2 core/shell nanostructures, and the SAXS patterns (PDF). This information is available free of charge via the Internet at http://pubs.acs.org.

CM801925J